

Winners and losers: Ecological and biogeochemical changes in a warming ocean

S. Dutkiewicz,^{1,2} J. R. Scott,^{1,2} and M. J. Follows¹

Received 30 August 2012; revised 1 April 2013; accepted 2 April 2013; published 20 May 2013.

[1] We employ a marine ecosystem model, with diverse and flexible phytoplankton communities, coupled to an Earth system model of intermediate complexity to explore mechanisms that will alter the biogeography and productivity of phytoplankton populations in a warming world. Simple theoretical frameworks and sensitivity experiments reveal that ecological and biogeochemical changes are driven by a balance between two impacts of a warming climate: higher metabolic rates (the “direct” effect), and changes in the supply of limiting nutrients and altered light environments (the “indirect” effect). On globally integrated productivity, the two effects compensate to a large degree. Regionally, the competition between effects is more complicated; patterns of productivity changes are different between high and low latitudes and are also regulated by how the supply of the limiting nutrient changes. These complex regional patterns are also found in the changes to broad phytoplankton functional groups. On the finer ecological scale of diversity within functional groups, we find that ranges of some phytoplankton types are reduced, while those of others (potentially minor players in the present ocean) expand. Combined change in areal extent of range and in regionally available nutrients leads to global “winners and losers.” The model suggests that the strongest and most robust signal of the warming ocean is likely to be the large turnover in local phytoplankton community composition.

Citation: Dutkiewicz, S., J. R. Scott, and M. J. Follows (2013), Winners and losers: Ecological and biogeochemical changes in a warming ocean, *Global Biogeochem. Cycles*, 27, 463–477, doi:10.1002/gbc.20042.

1. Introduction

[2] Phytoplankton communities in the sunlit layer of the surface ocean are important both as the base of the marine food web fueling fisheries and in regulating key biogeochemical processes such as export of carbon to the deep ocean. How will phytoplankton communities reorganize with changing climate? And how will this reorganization affect their productivity and ocean biogeochemistry? Models are a useful tool to investigate these questions. Here we employ a marine ecosystem model, with diverse and flexible phytoplankton communities which reorganize with changing climate, to examine what mechanisms might alter the biogeography and productivity of phytoplankton populations in a warming world.

[3] Temperature “directly” affects phytoplankton growth rates [Eppley, 1972; Bissinger *et al.*, 2008] impacting their

productivity and relative fitness. Warming and concurrent changes to the hydrological cycle and other climate properties will also alter the physical ocean circulation and mixing, “indirectly” impacting marine ecosystems by changing their light and nutrient environment. How do these two effects play out against each other in setting changes in phytoplankton communities and their productivity in the ocean? Here we employ a suite of numerical models along with a systematic theoretical framework to examine these two effects.

1.1. Biogeochemical Perspective

[4] Published numerical projections of future oceans suggest very different changes in global integrated primary production in future scenarios [Sarmiento *et al.*, 2004; Schmittner *et al.*, 2008; Steinacher *et al.*, 2010; Marinov *et al.*, 2010; Taucher and Oschlies, 2011; Bopp *et al.*, 2005; Bopp *et al.*, 2013], even disagreeing on the sign of the net change. Locally, there are only select regions of general agreement between models, with other regions of disparate signs of changes [Bopp *et al.*, 2013]. On the other hand, most numerical projections agree on the sign of the change in globally integrated export production, with better regional agreement as well. Why do models have such different responses at one metric of productivity but agree on another? Why are their responses so sensitive?

¹Department of Earth, Atmospheric and Planetary Sciences, Massachusetts Institute of Technology, Cambridge, Massachusetts, USA.

²Center for Global Change Science, Massachusetts Institute of Technology, Cambridge, Massachusetts, USA.

Corresponding author: S. Dutkiewicz, Department of Earth, Atmospheric and Planetary Sciences, Massachusetts Institute of Technology, 54-1412, 77 Massachusetts Ave., Cambridge, MA 02139, USA. (stephd@ocean.mit.edu)

[5] Model studies suggest that reduced rates of nutrient supply in a future ocean will lower productivity [Schmittner *et al.*, 2008; Steinacher *et al.*, 2010; Marinov *et al.*, 2010; Bopp *et al.*, 2013; Bopp *et al.*, 2001]. Taucher and Oschlies [2011], however, suggest that this “indirect” effect might be counteracted by the direct effect of increased growth rates due to increased temperatures. Here we more clearly separate the two effects with targeted sensitivity studies.

[6] Previous studies [e.g., Bopp *et al.*, 2001; Steinacher *et al.*, 2010; Marinov *et al.*, 2010] have suggested an opposite response in productivity between nutrient-rich high and oligotrophic low latitudes. Here we use simple theoretical insights to explore these regional differences further.

1.2. Ecological Perspective

[7] Previous model studies of global change [e.g., Bopp *et al.*, 2013; Steinacher *et al.*, 2010] have resolved only a handful of phytoplankton functional types. Most models include a small phytoplankton (characterized as slower growing but more efficient at low nutrient levels) and a large phytoplankton class (characterized as having higher maximum growth rates but reached only at higher nutrient levels). In this paper, we will refer to the former as “gleaners” and the latter as “opportunists.” Previous studies have suggested that reduced rates of nutrient supply in a future world will alter community structure to favor the gleaners (with their lower nutrient requirements) relative to the opportunists [e.g., Bopp *et al.*, 2005; Schmittner *et al.*, 2008; Steinacher *et al.*, 2010; Marinov *et al.*, 2010]

[8] Beyond this coarse-grained separation of functional groups, no other study has attempted to capture the finer-grained changes within community structure. The numerical model we employ here resolves major functional groups (which, as with previous models, can be loosely collected as gleaners and opportunists) and also a diversity within them, reflecting specific or ecotypic specialization in adaptation to temperature, light, resource availability, and predation. Here we employ this model to explore how a warming climate might impact marine phytoplankton communities and the range of species. What is the signature of global change from the ecological perspective?

[9] In our ecosystem model, diverse and flexible phytoplankton communities can reorganize with changing climate. We couple this model to an Earth system of intermediate complexity. We describe the numerical model in section 2 and the present-day results in section 3. We use the combination of sensitivity experiments and theory to explain changes in a warming world at the ecological level (section 4.1) and at the biogeochemical level (section 4.2).

2. Numerical Simulations

2.1. Earth System Model of Intermediate Complexity

[10] We use the MIT Integrated Global Systems Model (IGSM) framework [Dutkiewicz *et al.*, 2005a; Scott *et al.*, 2008; Sokolov *et al.*, 2009]. In this Earth system model of intermediate complexity, a three-dimensional ocean circulation module (MITgcm [Marshall *et al.*, 1997]) is coupled to a two-dimensional (latitude and height) atmospheric physical [Sokolov and Stone, 1998] and chemical module, and a terrestrial component [Schlosser *et al.*, 2007] with hydrology [Bonan *et al.*, 2002], vegetation

[Felzer *et al.*, 2004], and natural emissions [Liu, 1996]. The ocean has a horizontal resolution of $2^\circ \times 2.5^\circ$ and 22 vertical levels ranging from 10 m in the surface to 500 m at depth. Ocean boundary layer physics is parameterized following Large *et al.* [1994], and the effects of mesoscale eddies, not captured at this coarse resolution, is parameterized [Gent and McWilliams, 1990].

[11] The coupled system is spun up for 2000 years (using 1860 conditions) before simulating 1860 to 2100 changes. Atmospheric greenhouse gas and volcanic observations are specified from 1860 to 2000; for the 21st century, we use human emissions for a “business and usual” scenario that is projected by an economics module of the IGSM [Prinn *et al.*, 2011]. This scenario is constructed under the assumption that no climate policies are imposed over the 21st century and is similar to the Representative Concentration Pathways 8.5 (RCP8.5) used in the Coupled Model Intercomparison Project 5 (CMIP5).

[12] In the spin-up, historical, and future simulation phases, the three-dimensional ocean is forced with prescribed wind fields. These fields have variability as provided by the National Centers for Environmental Prediction (NCEP) [Kalnay *et al.*, 1996] reanalysis (detrended winds over the period 1948 to 2007 are employed; these winds are “recycled” for years outside this period), which drives interannual variability in the ocean model. For instance, an El Niño-Southern Oscillation (ENSO)-type signal is apparent. For simplicity, we do not represent changes to the wind patterns and intensity in the future period. Although some clear patterns of changes in wind stress emerge from analysis of the AR4 archive of coupled runs [Randall *et al.*, 2007], considerable model uncertainty remains [Yin, 2005; Fyfe and Saenko, 2006]. This aspect of physical changes to the system is beyond the scope of this work.

2.2. Marine Ecosystem Model

[13] We use the ecosystem model of Follows *et al.* [2007] with modifications [Dutkiewicz *et al.*, 2009; 2012] and direct the reader to those papers for full equations, parameter values, and discussion of the framework. Here we provide a brief overview and only the pertinent parameters (Table 1).

[14] We resolve inorganic and organic forms of nitrogen, phosphorus, iron, and silica, 100 phytoplankton types, as well as two grazers. The biogeochemical and biological tracers are transported and mixed by the climate system model and interact through the formation, transformation, and remineralization of organic matter. Excretion and mortality transfer living organic material into sinking particulate and dissolved organic detritus, which are respired back to inorganic form. Iron chemistry includes explicit complexation with an organic ligand, scavenging by particles [Parekh *et al.*, 2005], and representation of aeolian [Luo *et al.*, 2008] and sedimentary [Elrod *et al.*, 2004] sources.

[15] The time-dependent change in the biomass of each of the model phytoplankton types, P_j , is described in terms of a growth, sinking, grazing, other mortality, and transport by the fluid flow. Phytoplankton growth is a function of light, temperature, and nutrient resource. For phytoplankton type j (where $j = 1$ to 100), growth rate is given by the following:

$$\mu_j = \mu_{\max,j} \gamma_j^I \gamma_j^L \gamma_j^R \quad (1)$$

Table 1. Parameters of Phytoplankton Growth in the Ecosystem Model^a

Parameter	Symbol	Fixed Value	Random Assigned Values	Units
Max. growth rate at 30°C	μ_{maxj}	Small: 1.4 Large: 2.5		d ⁻¹ d ⁻¹
Temperature coefficient	A	-4000		K
Temperature range coefficient	B_j	Small: 0.001 Large: 0.0003		°C ⁻¹ °C ⁻¹
Temperature normalization coefficient	T_N	20		°C
Optimum temperature	T_{oj}		-2 to 35	°C
Temperature decay coefficient	b	4		
Temperature normalization coefficient	τ	0.33		
PAR saturation coefficient	k_{parj}		Small: mean 0.012, std 0.01 Large: mean 0.012, std 0.003	($\mu\text{Ein m}^{-1} \text{s}^{-1}$) ⁻¹ ($\mu\text{Ein m}^{-1} \text{s}^{-1}$) ⁻¹
PAR inhibition coefficient	k_{inhibj}		Small: mean 6×10^{-3} , std 1×10^{-4} Large: mean 1×10^{-3} , std 5×10^{-5}	($\mu\text{Ein m}^{-1} \text{s}^{-1}$) ⁻¹ ($\mu\text{Ein m}^{-1} \text{s}^{-1}$) ⁻¹
Phosphate half saturation	k_{PO_4j}	Small: 0.015 Prochl: 0.01 Large: 0.035		$\mu\text{M P}$ $\mu\text{M P}$ $\mu\text{M P}$
Nitrate half saturation	k_{NO_3j}	Small: 0.24 Large: 0.56		$\mu\text{M N}$ $\mu\text{M N}$
Ammonium half saturation	k_{NH_4j}	Small: 0.12 Large: 0.28		$\mu\text{M N}$ $\mu\text{M N}$
Silicic acid half saturation	k_{Si_j}	Non-diatom: 0 Diatom: 2.0		$\mu\text{M Si}$ $\mu\text{M Si}$
Iron half saturation	k_{Fe_j}	Small: 0.015 Prochl: 0.01 Large: 0.035		nM Fe nM Fe nM Fe

^a“Small” indicates gleaners, “large” indicates opportunists, “Prochl” indicates non-nitrate using *Prochlorococcus*-analogs, “Diatom” indicates silica-using phytoplankton type.

where μ_{maxj} is the maximum growth rate of phytoplankton j , and γ_j^T , γ_j^I , γ_j^R are the functions modulating growth due to temperature, light, and resource (nutrient) availability, respectively (Figure 1). See Appendix A and Dutkiewicz *et al.* [2009, 2012] for more details.

[16] The physiological functionality and sensitivity of growth to temperature, light, and ambient nutrient abundance (γ_j^T , γ_j^I , γ_j^R) for each of the hundred modeled phytoplankton type are governed by several true/false parameters, the values of which are based on a virtual “coin toss” at the initialization of each phytoplankton type. These determine the size class of each phytoplankton type (“large” or “small”), whether the organism can assimilate nitrate, whether the organism can assimilate nitrite, and whether the organism requires silicic acid. Some simple allometric

trade-offs are imposed: Phytoplankton in the large size class are distinguished by higher intrinsic maximum growth rates, faster sinking speeds, and higher half-saturation constants. This trade-off allows for the crude separation of the large “opportunists” adapted to highly seasonal, high-nutrient regions and the small “gleaners” adapted to low-nutrient, stable waters. In common with other ecosystem models, we also parameterize the opportunists through their larger size and sinking speed as exporting carbon to the deep ocean more efficiently [Pomeroy, 1974; Laws, 1975]. We do not include parameterization of nitrogen fixation in these simulations.

[17] Parameter values which regulate the effect of temperature and light on growth (T_{oj} , k_{parj} and k_{inhibj}) are assigned stochastically, drawn from broad ranges guided by

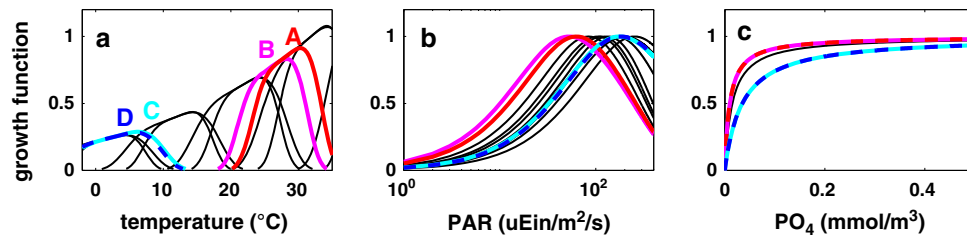


Figure 1. Functional forms of the sensitivity of phytoplankton growth to (a) temperature (γ_j^T); (b) flux of photosynthetically active radiation (γ_j^I), and (c) ambient resource concentration (γ_j^R), here specifically for phosphate. The collection of curves in each panel is chosen to illustrate the ranges from which initialized growth sensitivities are selected. At any time and location, each phytoplankton type has a realized growth given by $\mu_j = \mu_{maxj} \gamma_j^T \gamma_j^I \gamma_j^R$ (equation (1); see Appendix A for more details). Larger phytoplankton are given a higher intrinsic growth rate, μ_{maxj} , and higher nutrient half saturation (see Table 1). Colored curves and letters refer to the phytoplankton types shown in Figures 4, 5, and 6. Though difficult to see at this scale, phytoplankton type C has a higher optimum temperature and a lower light optimum than D.

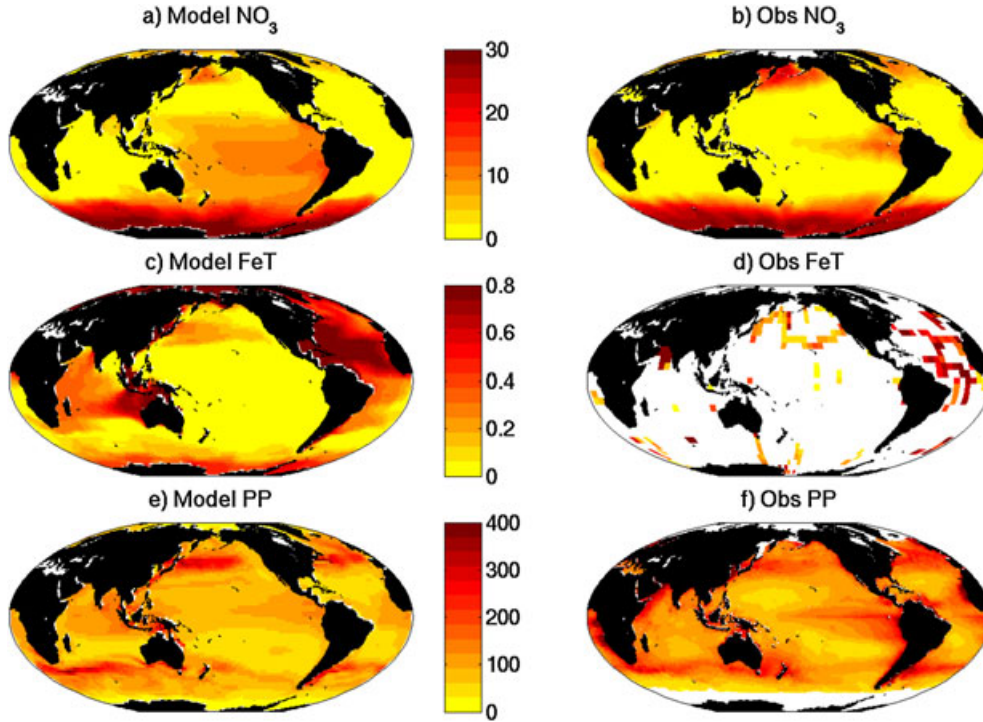


Figure 2. Biogeochemistry and productivity. (a) “Present-day” model nitrate in surface 50 m (mmol N m^{-3}); (b) nitrate in surface 50 m (mmol N m^{-3}) from observations (World Ocean Atlas [Garcia *et al.*, 2006]); (c) present-day model iron in surface 50 m ($\mu\text{mol Fe m}^{-3}$); (d) observed iron ($\mu\text{mol Fe m}^{-3}$) from the compilation of Moore and Braucher [2008], white indicates no data; (e) present-day model primary production ($\text{gC m}^{-2} \text{y}^{-1}$) over surface 50 m; (f) primary production ($\text{gC m}^{-2} \text{y}^{-1}$) derived from satellite measurements [Behrenfeld and Falkowski, 1997].

laboratory and field studies (Table 1). In particular, each phytoplankton type was randomly assigned an optimal temperature for growth and was only viable over a specified temperature range (Figure 1a).

[18] The phytoplankton are grazed by two zooplankton size classes. Large zooplankton preferentially graze on large phytoplankton but can graze on small phytoplankton, and vice versa for small zooplankton.

[19] Primary production (PP) is a function of growth rates (hence nutrient, light, and temperatures) and phytoplankton biomass:

$$\text{PP} = \sum_j \mu_{\max j} \gamma_j^T \gamma_j^I \gamma_j^R P_j \quad (2)$$

[20] Export production (EP) is defined here as particulate inorganic carbon (POC) sinking through 100 m at rate w ,

$$\text{EP} = w \frac{\text{dPOC}}{\text{dz}} \quad (3)$$

where POC is a function of PP and also the type of community present, since large phytoplankton are parameterized as providing more to the sinking POC pool than small phytoplankton.

2.3. Experiment Design

[21] We use the physical fields of the three-dimensional ocean component of the IGSM to drive the biological and

biogeochemical fields of the ecosystem model. In particular, we use the three-dimensional temperature, circulation vectors (meridional, zonal, and vertical fluid flow), mixing parameters, and sea-ice cover fields. The surface photosynthetically available radiation is provided by monthly mean SeaWiFS products, and the monthly surface iron dust is from the model of Luo *et al.* [2008]. These latter two fields are climatological means and do not change in the simulations described here. Though the impact of changes in light and dust are likely to be important in the future, they are beyond the scope of this paper.

[22] Nutrient distributions were initialized from output from previous simulations, though the key results presented here are not sensitive to these initial conditions. The 100 phytoplankton were all initialized with the same low initial condition.

[23] Since it is computationally expensive, the ecosystem simulations are run for only 200 years. The first 100 years used present-day conditions (1995–2005 repeating) to quasi-spin-up the ecosystem and biogeochemical fields. A repeating seasonal cycle is quickly reached, and there is only a small biogeochemical drift associated with upwelling of deep water. The several thousand years of integration needed to adjust the deep ocean is computationally unfeasible. After a few years’ adjustment during this initial spin-up, the biomass of about a third of the 100 phytoplankton types fell below the threshold of numerical noise, and these types were assumed to have become “extinct.”

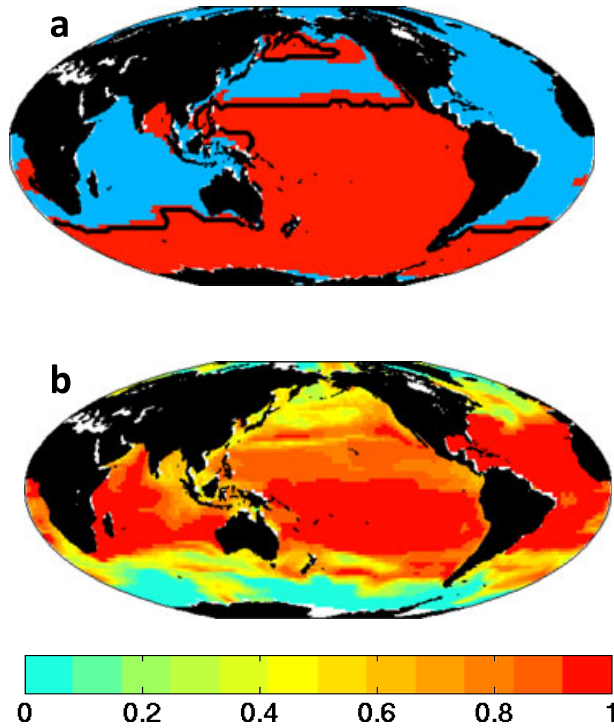


Figure 3. (a) Limiting nutrient to phytoplankton growth. Color indicates present-day conditions: Red represents limitation by iron, and blue dissolved inorganic nitrogen. The black line indicates the boundary between these regions in year 2100 from *All*. (b) Fraction of gleaners relative to total biomass in present day.

[24] From the quasi-equilibrium state, we conduct several different experiments, each for an additional 100 years:

[25] 1. *Control*. For another 100 years, the 1995–2005 conditions are sequentially cycled. This experiment provides a measure of the biogeochemical/ecological drift (small) and a baseline from which to compare the climate change experiments.

[26] 2. *All*. The temperature, circulation, mixing, and sea-ice fields change as projected by the Earth system model from 2000 to 2100.

[27] 3. *Direct*. The temperature fields that affect biological rates are allowed to change from 2000 to 2100, but the circulation, mixing, and sea-ice fields repeat 1995–2005. This experiment therefore highlights the “direct” effect of warming on phytoplankton growth rates alone.

[28] 4. *Indirect*. Temperature fields repeat 1995–2005 for 100 years, but the circulation, mixing, and sea-ice fields are allowed to change as for 2000–2100 conditions. This experiment therefore highlights the “indirect” effects of changes to light environment and nutrient supply.

[29] 5. *Indirect-ice*. Temperature fields, circulation, and mixing fields repeat 1995–2005 for 100 years, but sea-ice fields are allowed to change as for 2000–2100 conditions.

[30] 6. *Indirect-circ*. Temperature fields and sea-ice fields repeat 1995–2005 for 100 years, but circulation and mixing fields are allowed to change as for 2000–2100 conditions.

[31] In previous studies with this ecosystem model approach with random assignment of traits [Follows *et al.*,

2007; Dutkiewicz *et al.*, 2009; Barton *et al.*, 2010], we have conducted an ensemble of simulations, each member with a different randomization of the physiological parameters. In those studies, we have found global integrated values (such as global primary production); regional patterns of biomass, productivity, and diversity; and range of functional types of phytoplankton to be robust between ensemble members. Here with several hundred years of integration (and several sensitivity experiments), it was not feasible to run a large ensemble. Instead we conduct only one other “ensemble member.” In this additional simulation, with a different randomization of physiological parameters, the first 100 year quasi-spin-up was completed, and then analogs of the *Control* and *All* experiments were conducted. In the results discussed below, we highlight those changes that are robust between these two ensemble members.

3. Present-Day Conditions

[32] Experiment *Control* provides a “present-day” baseline from which to compare the climate change experiments. The biogeochemistry, productivity (Figure 2), ecosystem community structure, and diversity in the simulated present-day ocean were qualitatively reasonable and similar to those found in earlier studies using this ecosystem model [Follows *et al.*, 2007; Dutkiewicz *et al.*, 2009; Barton *et al.*, 2010; Saba *et al.*, 2010]. Iron measurements are still sparse, but the model qualitatively captures the observed gradients between major ocean basins [Parekh *et al.*, 2005; Dutkiewicz *et al.*, 2005b]. We do not adequately resolve coastal processes, underestimating productivity near shore. The model also has lower productivity in the equatorial Pacific than observed, possibly due to iron supply which is too low here. As a consequence, local nitrate levels are too high. The model does however capture the broad patterns of low nutrients and

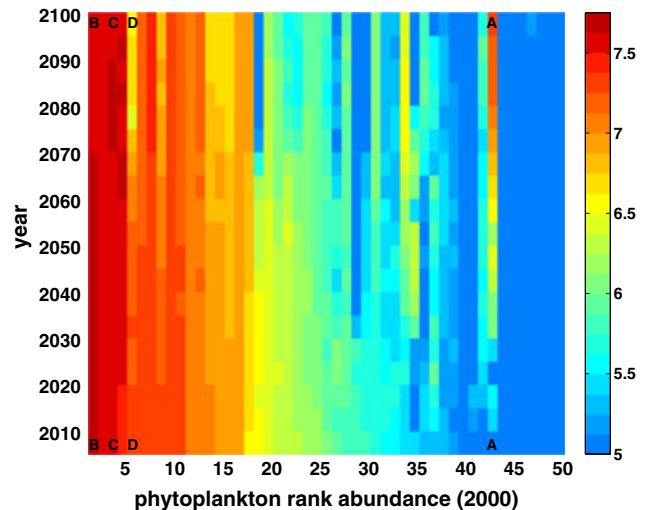


Figure 4. Phytoplankton type global biomass as a function of year from experiment *All*. Shown are the 50 most abundant phytoplankton types arranged in order of their annually averaged globally integrated biomass (“rank abundance”) in year 2000 (GtC, logarithmic scale). Letters indicate the four phytoplankton types shown in Figures 1, 5, and 6.

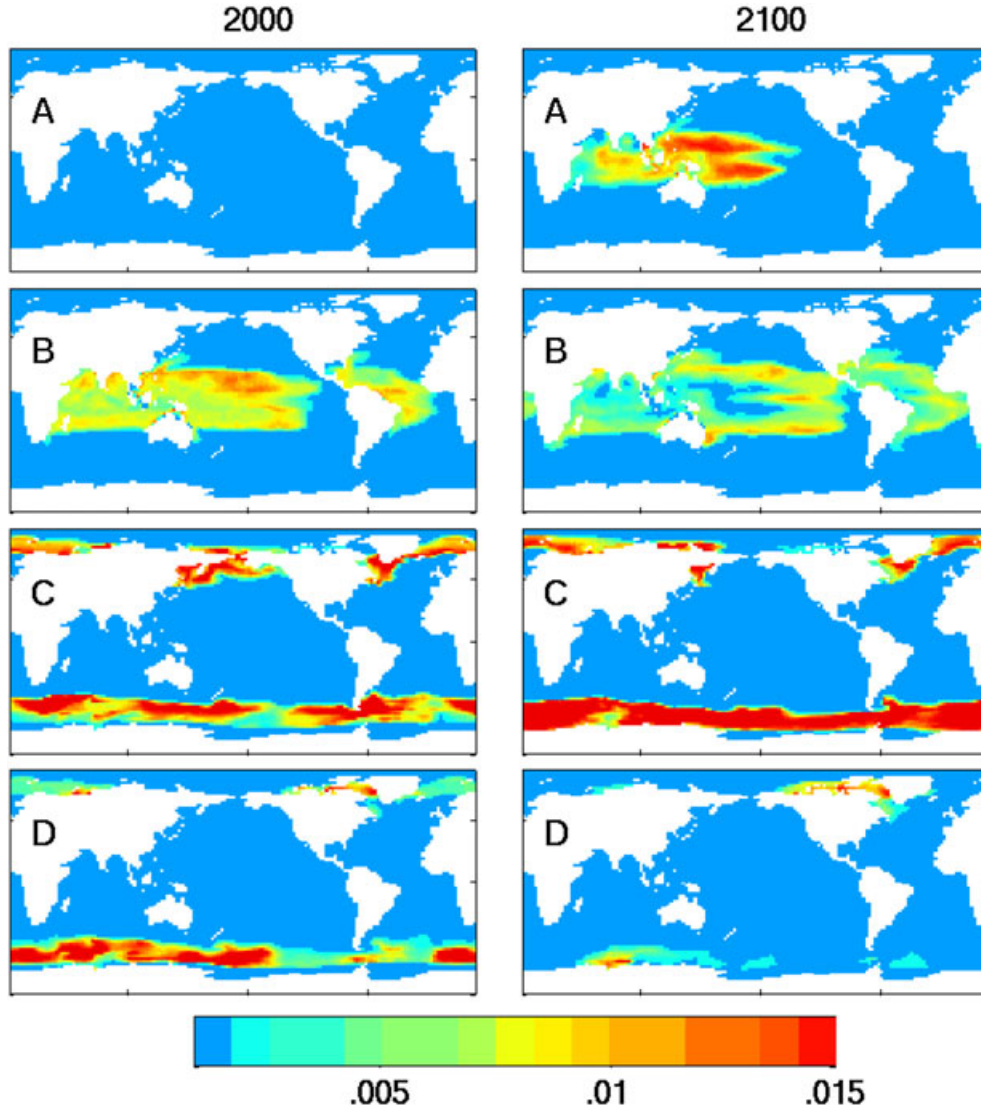


Figure 5. Ecological perspective: Changing phytoplankton ranges in *All*. The distribution of four (of the 100) phytoplankton types shown as annual mean biomass concentration over top 50 m (gC m^{-3}). Panels on the left are the 2000 conditions; the right panels show the same phytoplankton at year 2100. Letters correspond to the types also highlighted in Figures 1, 4, and 6.

productivity in the subtropical gyres and higher productivity and nutrients in the high latitudes and upwelling equatorial regions. Iron limitation of growth (Figure 3a) is found in the classic “High Nitrate, Low Chlorophyll” (HNLC) regions: the Southern Ocean, equatorial Pacific and northern Pacific. All other regions of this simulation are limited by dissolved inorganic fixed nitrogen.

[33] Most of the global biomass comprises about 20 phytoplankton types but with minor contributions from a long tail of rarer types (bottom row of Figure 4). The abundance ranking is not constant over time, even under present-day conditions of *Control*, shifting with season and with interannual variability that is imposed on the model.

[34] Two theoretical ecological regimes (Dutkiewicz *et al.* [2009], further outlined in Appendix B) provide a rationale for separation of biomes dominated by gleaners and opportunists (Figure 3b). The amount of seasonality suggested by the annual range of the mixed layer depth provided a good

metric to separate the two biomes [Dutkiewicz *et al.*, 2009]. The strongest gradient of this mixed layer depth range is found at about 40° North and South, and we use this as a dividing line here.

[35] In the regions of low seasonality (nominally equatorward of 40°), coexisting phytoplankton types have similar R^* , a combination of physiological traits [Tilman, 1977; Dutkiewicz *et al.*, 2009; Barton *et al.*, 2010]

$$R_j^* = \frac{k_{R_j} m_j}{\mu_{\max_j} \gamma_j^T \gamma_j^I - m_j}$$

where k_{R_j} is the nutrient half-saturation coefficient and m_j is the phytoplankton loss term (see Appendix B, equation (B3)). In these more stable environments, “gleaners” tend to win out over the larger opportunists, as their combined maximum growth, μ_{\max_j} , and half saturation for nutrients, k_j , lead to lower R_j^* . Here the gleaners are all provided the same μ_{\max_j} , though those that can fix

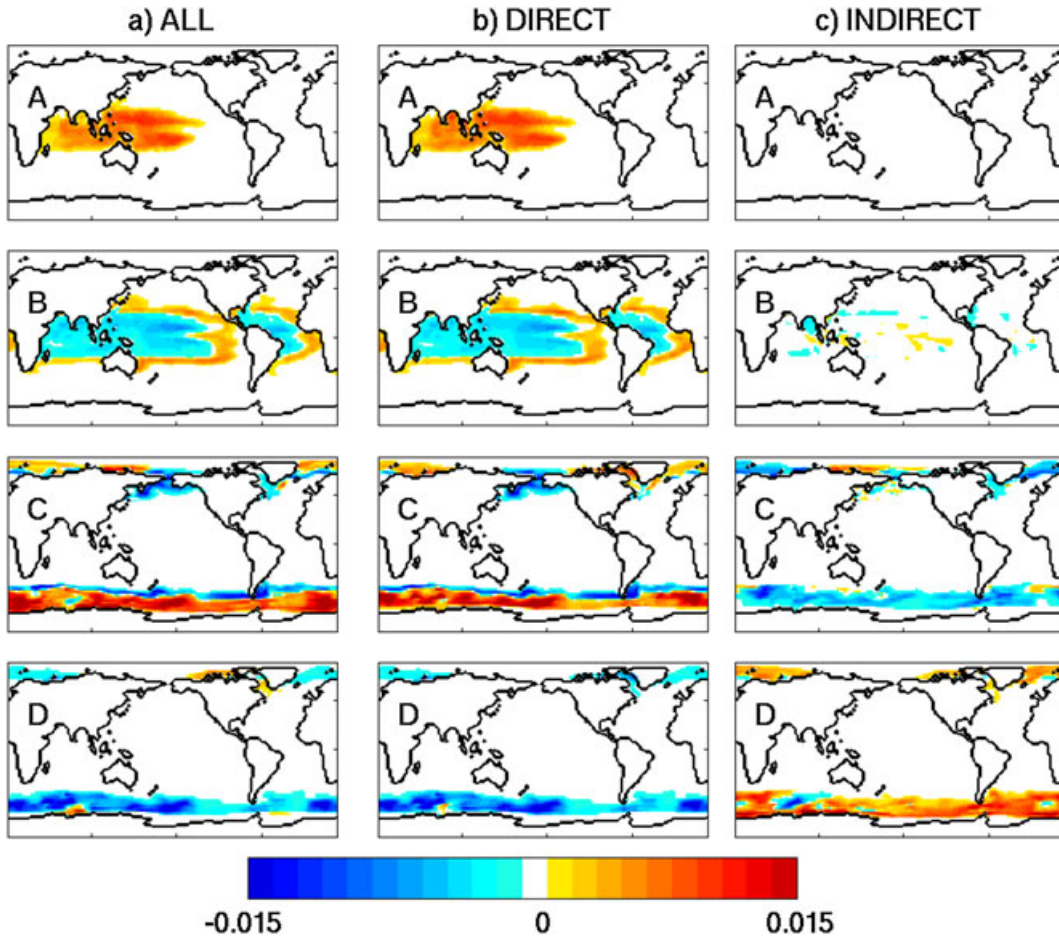


Figure 6. Ecological perspective: Changing phytoplankton ranges. Difference between phytoplankton biomass (gC m^{-3}) of four (of the 100) phytoplankton types shown in Figure 5. This is the difference between 2100 and 2000 for (a) *All*, (b) *Direct* (experiment highlighting only the impact of warmer temperature on biological rates), and (c) *Indirect* (experiment highlighting only the indirect effects of changing physical environment on nutrient and light environment). Red indicates a local increase in phytoplankton type biomass in 2100 relative to 2000, blue a decrease.

nitrate have slightly larger k_j than those that do not (see Table 1). The combination of the temperature and light preferences (γ_j^T, γ_j^I) is therefore instrumental in setting which of the gleaners has the lowest R_j^* . Those types with the lowest R^* draw the nutrients down to this value [Tilman, 1977; Dutkiewicz et al., 2009] and exclude all others, in particular those with non-optimal γ_j^T, γ_j^I . Our model therefore captures a finer-scale resolution of gleaner coexistence, with the specific ranges (e.g., Figure 5, types A and B) defined by the individual-type temperature and light preferences. In this case, type A is adapted to higher temperatures than type B is (Figure 1) and has only a very small and very low abundance relative to B in present-day conditions (Figure 5, left column).

[36] The theoretical framework (Appendix B) suggests that in the high latitudes growth rate alone is important in determining which type dominates. In the high seasonality regions, the “opportunists” which have a higher $\mu_{\max j}$ are indeed more abundant (Figure 3b) with those types with highest local growth rate dominating. Since all opportunists in this model have the same $\mu_{\max j}$, dominance between opportunists is also dictated by the local modification on

growth rate by γ_j^T and γ_j^I . For instance, type C is adapted to higher temperatures than D (Figure 1) and therefore has a range more equatorward (Figure 5, left column).

[37] We note that the separation between gleaners and opportunists is not well demarcated (Figure 3b). Top-down control [Prowse et al., 2012a; Ward et al., 2012] by two grazers (who preferentially prey on either gleaners or opportunists) and continual mingling of populations by advection and mixing allow for greater degree of diversity.

[38] In the difference relative to “2000” discussed in the remainder of this paper, we show variables relative to the appropriate year of this *Control* experiment. This removes the minor biogeochemical drift from the results and is a technique used frequently in presenting climate change experiments.

4. Perturbed System

[39] In the “business as usual” scenario presented here, the model marine ecosystem is perturbed from its present-day state by the altered physical ocean resulting from the projected anthropogenic emission of greenhouse gases

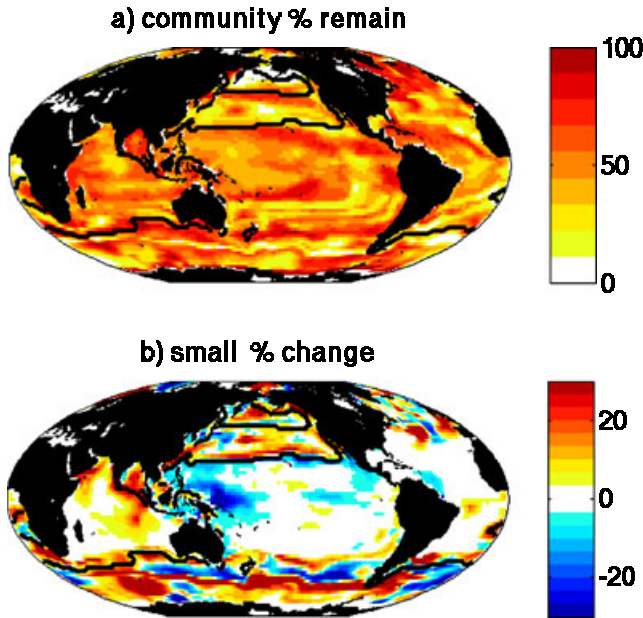


Figure 7. Ecological perspective: Changes between 2000 and 2100 in the top 50 m of *All*: (a) 2000 local community remaining (equation (4), % indicates amount of biomass of original community that survives; note though that other phytoplankton types may have invaded, so this does not reflect change in total biomass); (b) total biomass made up of small gleaner phytoplankton (increase indicates biomass is made up of more gleaners relative to opportunists than in year 2000). Black contour indicates boundary between regions where majority of biomass is limited by availability of iron or dissolved inorganic nitrogen (Figure 3a).

[Sokolov *et al.*, 2009] and associated climate change. The atmospheric $p\text{CO}_2$ at year 2100 is 1300 ppmv, global mean surface air temperature has increased by 5°C , and the mean global sea surface temperature has increased by 3°C (varying between 0 and 5°C). There is larger increase in the Northern Hemisphere due to the presence of landmasses. On these time scales, the heat that enters the ocean has not had a chance to redistribute evenly; more is trapped near the surface, leading to increased stratification and reduced mixing at the surface. Sea-ice retreats. The meridional overturning circulation slows and shallows relative to 2000 conditions. The reduced surface mixing and shifts in the meridional overturning lead to an increased separation of the surface waters from the deep, reducing the supply of macronutrients from depth, at least over the time scales addressed in this paper [Schmittner, 2005].

[40] How do these physical changes impact the phytoplankton? The suite of experiments described in section 2.3 is designed to separate the direct and indirect responses to this warming world. We will discuss separately the changes on the ecosystem biogeography and community level and the changes on the biogeochemical productivity level.

4.1. Ecological Changes

[41] The ranges of individual phytoplankton types change significantly over the course of the hypothetical 21st century (Figures 5 and 6a), shifting poleward and, in lower latitudes,

eastward. We interpret the shifts in these ranges using the theoretical framework.

[42] As an example, in the low-latitude warm pool region, phytoplankton type B dominated in 2000 (Figure 5): this gleaner type had the optimal combination of γ_j^T and γ_j^I and thus the lowest R_j^* . However, as temperatures increased over the course of the hypothetical 21st century, in this region γ_B^T decreases (see Figure 1), leading to a higher R_B^* (equation (B3)). At the same time, for type A, γ_A^T increases in this region, leading to a lowering of its R_A^* . Eventually, R_A^* becomes smaller than R_B^* , and type A takes over as dominant. However, just poleward (and eastward) of this warm

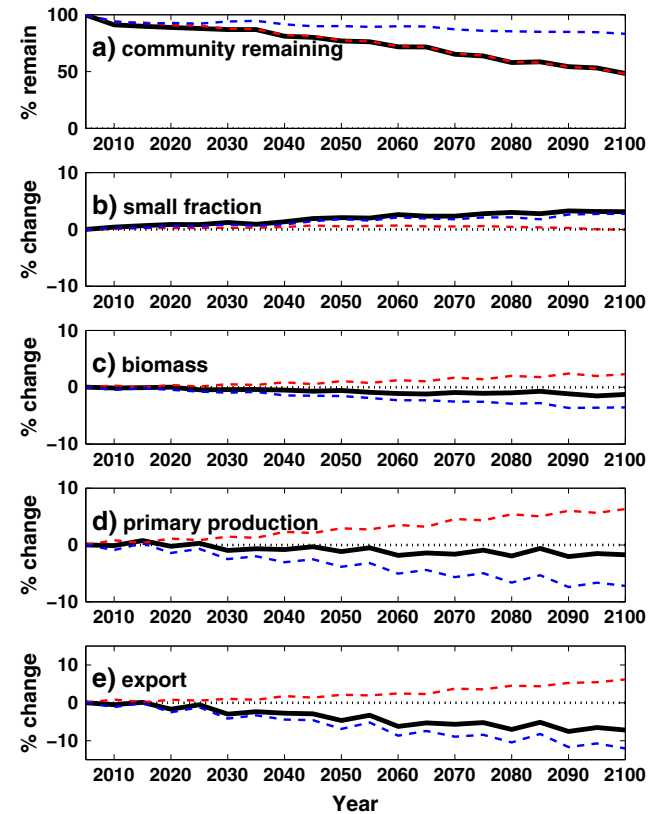


Figure 8. Globally integrated properties in warming scenario relative to 2000 values. (a) Percent of 2000 local community remaining (equation (4), % indicates amount of biomass of original community that survives; note though that other phytoplankton types will have invaded, so this does not reflect the changes to total biomass); (b) change in the percentage of total biomass made up of small gleaner phytoplankton (positive values indicate biomass is made up of more gleaners relative to opportunists than in year 2000); (c) percentage change in biomass; (d) percentage change in primary production (PP); (e) percentage change in export production (EP) as defined as the rate of sinking particulate carbon through 100 m. Black solid line indicates experiment *All*, red dashed line indicates results from experiment highlighting only the impact of warmer temperature on biological rates (*Direct*), and blue indicates experiment highlighting only the indirect effects of changing physical environment on nutrient and light environment (*Indirect*). Black dotted line indicates zero.

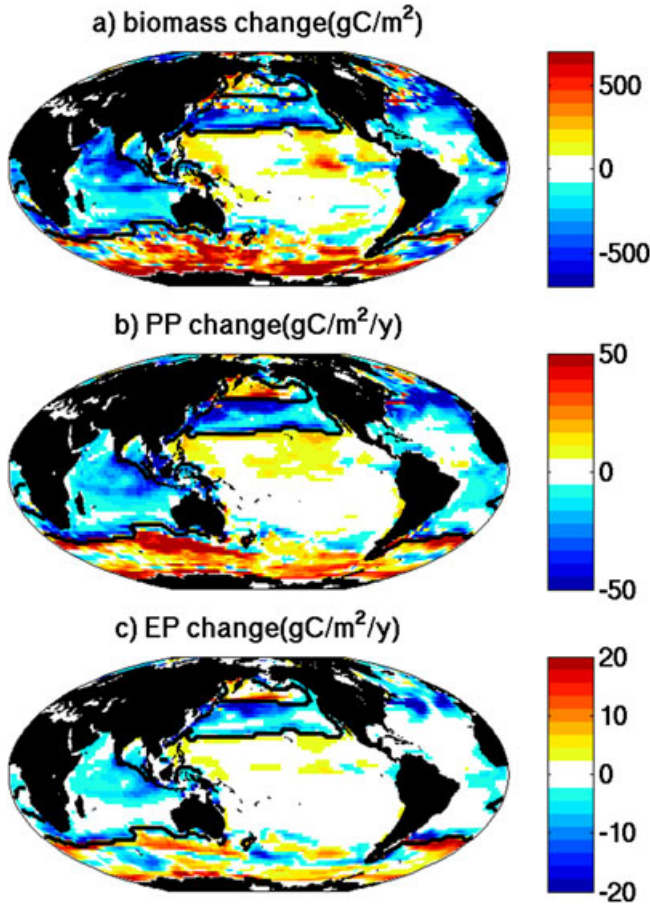


Figure 9. Biogeochemical perspective: Changes between 2000 and 2100 for *All*: (a) biomass (gC m^{-2}); (b) primary production (PP) ($\text{gC m}^{-2} \text{y}^{-1}$); (c) export production (EP) defined as rate of sinking particulate carbon through 100 m ($\text{gC m}^{-2} \text{y}^{-1}$). Red indicates an increase in 2100 relative to 2000, blue a decrease. Black contour indicates boundary between regions where majority of biomass is limited by availability of iron or dissolved inorganic nitrogen (Figure 3a).

pool region, the water temperatures are also rising—here temperatures become more favorable for type B; in these new regions, R_b^* becomes lower than the type that dominated in those regions in 2000. The range of type B shifts into these waters. Thus, locally B “loses” in some regions but will “win” in others.

[43] The model sensitivity experiments *Direct* and *Indirect* show that the shift in ranges of A and B are driven primarily by temperature changes (Figure 6b) and less by changes in light environment (Figure 6c). The global total biomass of A increases from insignificant to a major player over the course of the 100 year warming (Figure 4). However, though the global total biomass of B does decrease (Figure 4), it does not drop below the biomass of type A over the course of this hypothetical 21st century. Thus, globally B is not a significant “loser.”

[44] In the high latitudes, a similar shifting of ranges occurs (e.g., types C and D, Figure 5), driven by changes to γ_j^T and γ_j^D and their impact on growth rates. Type C moves

poleward as waters there approach the optimum in its γ_C^T , while D is out-competed as its γ_D^T decreases. In these most poleward regions, there is no further habitat with temperatures that can accommodate D. Thus, D both locally and globally “loses” (Figures 5 and 4). In this example, the changes to temperature and light environments have opposite effects: the more stratified conditions favor the higher light-adapted type D over type C (Figure 6c), though the temperature-driven changes dominate in *All*.

[45] All ranges shift, but some types have increased (e.g., A, C) and some decreased (e.g., D) areal extent. Habitats do not shift completely but have regions that overlap for 2000 and 2100 conditions (e.g., B, C, D); it is the margins that shift. Shifts to some regions may in fact be beneficial to some phytoplankton types. For instance, the extent of type B shifts southward in the South Pacific Ocean; and in these new regions, the biomass appears to have increased relative to earlier values when it inhabited regions further to the north. We can explain this looking at equation (B5). Phytoplankton biomass is a function of the supply of the limiting nutrient, S_R . Type B’s new range incorporates waters with higher nutrient supply than its previous range to the north, thus leading to higher biomass supported in this new region. Thus, it is the combined change in areal extent and change in regionally available nutrients that leads to global “winners and losers” (Figure 4). Interestingly, these “wins” can be transient. For instance, type C (Figure 4) has an increasing global biomass through the 2080s but near the end of the century begins to decline.

[46] At any location, several phytoplankton types coexist: Each location has a community structure. How much does this community structure change with hypothetical future warming? We see that ranges shift, so that new phytoplankton types invade a new location. However, we also note that ranges do not shift completely to new areas but have overlapping extents between present-day and 2100 conditions. To gain an appreciation of the mixture of plankton types, we calculate a measure of community structure change:

$$C_s(t) = 100 \times \sum_1^J \min \left(\frac{P_j(t)}{\sum_1^J P_j(t_0)}, \frac{P_j(t_0)}{\sum_1^J P_j(t_0)} \right) \quad (4)$$

where t_0 is present day. If the community did not change at all at time t , then $C_s(t) = 100\%$. If all phytoplankton types increased, then $C_s(t)$ is still 100%: The original community is still there, but there is additional biomass. But if any phytoplankton types had decreased biomass, then $C_s(t) < 100\%$. The lower $C_s(t)$, the more of the original community has disappeared from that location (though total biomass may or may not have changed). In the scenario presented here, the local community at 2100 was composed of about only half the community that was there in 2000 (see Figures 7a and 8a) consistently across regions. Most of the shift in local community was attributed primarily to the direct impact of warming on the phytoplankton growth rates (*Direct*, red line in Figure 8a): This is driven by shifts in the ranges. Globally there is a smaller but significant shift in community structure from the indirect effect (blue line), mostly a consequence of the reduced supply of nutrients from depth.

[47] Globally, the shifts in community structure favor the gleaner populations (Figure 8b). Here we show the percentage of the total biomass that is made up of gleaners. Note

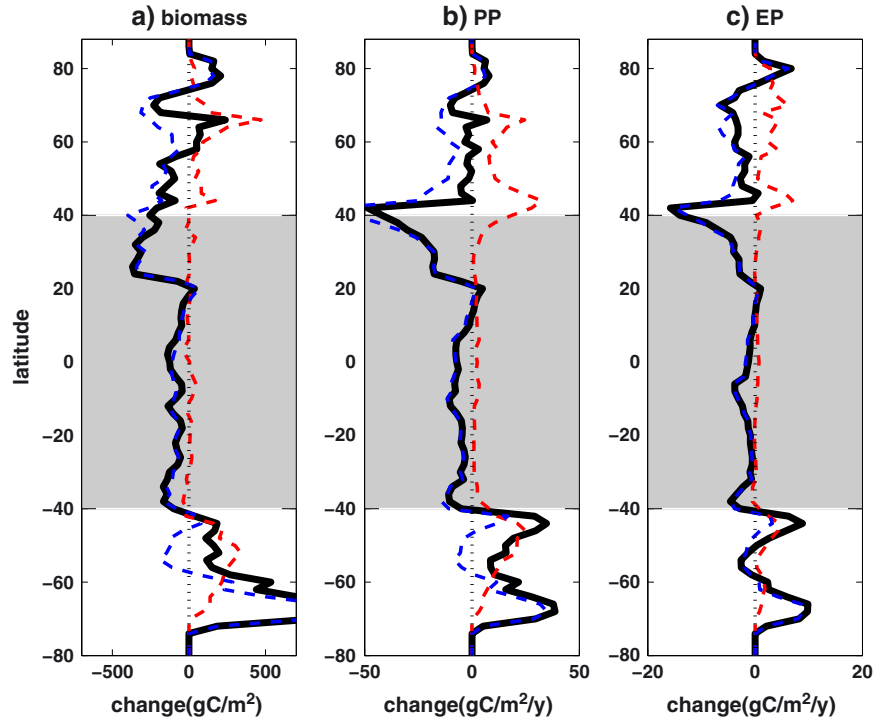


Figure 10. Biogeochemical perspective: Zonally averaged changes between 2000 and 2100: (a) biomass (gC m^{-2}); (b) primary production (PP) ($\text{gC m}^{-2} \text{y}^{-1}$); (c) export production (EP) defined as rate of sinking particulate carbon through 100 m ($\text{gC m}^{-2} \text{y}^{-1}$). Black solid line indicates experiment *All*, red dashed line indicates results from experiment highlighting the impact of warmer temperature on biological rates (*Direct*), and blue indicates experiment highlighting the indirect effects of changing physical environment on nutrient and light environment (*Indirect*). Black dotted line indicates zero; gray shading indicates region where resource competition theory is most applicable [Dutkiewicz *et al.*, 2009]; see Appendix B.

that this does not take into account the change in biomass (discussed later) but considers merely the relative community structure. Globally, the relative abundance of gleaners increases almost exclusively from the indirect effect (Figure 8b) of reduced nutrient supplies as noted by several earlier studies [Bopp *et al.*, 2005; Steinacher *et al.*, 2010; Marinov *et al.*, 2010]. This is especially true in mid and higher latitudes as more stratified, more stable conditions favor small phytoplankton (Figure 7b). However, unlike the strong and global pattern of changes in community structure, this “functional” level change in the ecosystem is regionally more complex with patterns of increases and decreases. Some patterns of increase/decrease come from shifts in temperature fronts (e.g., Southern Ocean), but others are more complex. We will discuss these further in the next section.

4.2. Changes at the Biogeochemical Level

[48] As found by many (but not all) previous studies, there is a global decline in phytoplankton biomass and primary and export production over the 100 years (Figure 8), but the regional patterns are complex (Figure 9). To visually separate out the direct and indirect effects on these biogeochemical variables, we present zonally averaged changes (Figure 10).

[49] Our theoretical framework (see Appendix B) for oligotrophic regions with low seasonality suggests that total

phytoplankton biomass is determined by the ratio of the rate of supply of the limiting nutrient and the phytoplankton loss rates (equation (B5)) and not by the growth rates of the phytoplankton present. In experiment *Direct* (red line, Figure 10a), where nutrient supply rates do not change, there is little change in biomass in these regions between present day and 2100, even though the community structure had changed significantly (Figure 7a). In experiment *Indirect* (blue line, Figure 10a), there is a zonally averaged reduction in biomass linked to decrease in the macro nutrient nitrate supply (S_R) from the deep ocean. The indirect effect therefore dominates in these low-latitude regions, but its impact differs between regions where growth is limited by nitrate and those limited by the micronutrient iron (Figure 9a). Atmospheric delivery of dust is a major source of iron to the ocean, and in this model the dust supply does not change. Though iron is also supplied from depth, in the subtropical regions lateral supplies are more important [Dutkiewicz *et al.*, 2005b]. An increase in biomass occurs in regions where lateral iron supply from upstream becomes higher. These upstream regions are nitrate limited and therefore have a reduction in biomass. There is a subsequent reduction in the drawdown of iron, allowing more to be laterally transported to the iron-limited regions. This also leads to a relative increase in opportunist in these regions (Figure 7b). It is, however, likely that atmospheric delivery of iron will change with climate and would impact the ecological and

biogeochemical dynamics discussed above. Projections of changes to iron deposition in the future are uncertain [Tegen *et al.*, 2004; Luo *et al.*, 2008; Mahowald and Luo, 2003].

[50] At higher latitudes, our theoretical framework suggests that increased growth rate alone would lead to higher biomass and more efficient drawdown of nutrients. In the highest latitudes (poleward of about 70°), increased growth rates and reduced sea-ice cover (captured in *Indirect* but not in *Direct*) also leads to increased biomass (Figures 9a and 10a and as demonstrated in additional experiments *Indirect-ice* and *Indirect-circ*, not shown here). However, between latitudes 40° and 70°, there is a competition between increased growth rates and reduced rate of nutrient supply. Increase in biomass in the iron-limited regions (Southern Ocean and North Pacific) indicates that the direct effect wins out when the limiting nutrient supply rate is relatively unchanged (Figure 9a). In the nitrogen-limited North Atlantic, reduced nitrate supply rates (important after seasonal drawdown even in these high-nutrient supply regions) win out, and there is a reduction in biomass (Figure 9a).

[51] The interplay between increases in biomass in some high-latitude regions, where the direct effect wins out, and the general decrease in most low-latitude regions, where the indirect effect of reduced supply rates is most important, leads to a delicate global balance in changes to total biomass (Figure 8c).

[52] We see a broad similarity between the global and regional responses of primary production and biomass (Figures 8d, 9b, and 10b). However, since primary production is a product of both biomass and growth rate (and thus temperature; see section 2, equation (2)), the competition between the direct and indirect effects are even more important. In low latitudes, the temperature dependence of growth allows for a slight increase in *Direct*, though this is offset by the reduction of supply of macronutrients in *All* (Figure 10b). But similarly with biomass, in some low-latitude regions with increased lateral supply of iron, there can be an increase in primary production (Figure 9b). Globally integrated, the direct and indirect effects on primary production are opposing and almost compensating (Figure 8d).

[53] The biological export of carbon from the surface ocean to the deep is regulated by both the primary production and the phytoplankton community structure. The model results show a shift to relatively more gleaners which are modeled to drive export of carbon less efficiently. Since the indirect effect of warming through reduced nutrient supply leads to both a decrease in primary production in this model and a shift toward a relatively larger fractional biomass of gleaners, this effect wins out over the direct effect (Figure 10c), and there is global reduction in export of carbon (Figure 8e).

5. Discussion and Summary

[54] Here we have employed a numerical model to tease apart how some aspects of a warming ocean may impact competition and productivity in phytoplankton. Our model does not represent, for example, changing to dust (iron) deposition [Tegen *et al.*, 2004; Luo *et al.*, 2008; Mahowald and Luo, 2003], acidification [Doney *et al.*, 2009], flexible elemental composition of phytoplankton [Tagliabue *et al.*,

2011], or nitrogen fixation. Additional levels of complexity in the grazer parameterizations will affect the diversity [Prowe *et al.*, 2012a; Ward *et al.*, 2012] and productivity [Prowe *et al.*, 2012b]. Such processes and additional sensitivities will make predictions even more complex and the underlying mechanisms more difficult to pull apart. Here we have limited ourselves to prying apart the differing effects of direct changes to phytoplankton growth rates and the indirect effects of the warming on their nutrient and light environment. We find that the ecological and biogeochemical responses are complex and can be transient and that there is a delicate balance between these two effects.

5.1. Biogeochemical Perspective

[55] Biogeochemically, the direct and indirect effects of warming can be in opposition and largely compensate on a global scale (Figures 8c and 8d) as suggested by Taucher and Oeschies [2011]. However, in that study, two ecosystem models were used: one with a temperature dependence on growth and the other without. We argue here that our sensitivity studies (*Direct* and *Indirect*) with the same ecosystem provide a cleaner and more consistent method to examine the interplay of these two effects and in particular the regional competition (Figure 10). The theoretical framework provides a rationale for the impact of reduced nutrient supply (indirect effect) being most pronounced on biomass and primary productivity at lower latitudes, with increased growth rates (direct effect) playing a stronger (but not necessarily dominant) role in nutrient-rich higher latitudes. These findings are consistent with and extend on those of previous studies [e.g., Bopp *et al.*, 2001; Steinacher *et al.*, 2010; Marinov *et al.*, 2010]. Here we also show that these results are modulated by whether growth is limited by supply rate of iron or macronutrients (Figure 9). Though our results are dependent on our crude assumption of a non-changing aeolian dust field, they do indicate that complex upstream effects and changes in lateral supplies of nutrients will alter local changes in productivity. The regional changes to biomass and primary production will be highly complex, with some regions “winning” and some “losing.”

[56] There is a delicate balance globally between the direct and indirect effects on primary production (Figure 8d). We suggest that the uncertainty in net change of modeled biomass and primary productivity [e.g., Sarmiento *et al.*, 2004; Steinacher *et al.*, 2010; Bopp *et al.*, 2013] can be understood by variations in the competition between the two effects which depend on intermodel differences in the parameterization of growth (and its temperature dependence) and the extent of the physical changes to the ocean.

[57] A recent intercomparison of CMIP5 RCP8.5 simulation [Bopp *et al.* 2013] found that 10 different models agreed on a local decrease in primary production in the tropical Indian, tropical Western Pacific, tropical Atlantic, and North Atlantic (consistent with our model results, Figure 9b). The CMIP5 models did not agree however on the sign of change of primary production over most of the rest of the ocean. We can use the mechanistic insight gained from this study to speculate why robust answers between models only occur in some regions. We note that all the regions of robust response are strongly nitrogen limited in our model. All models (ours and the CMIP5) simulate a reduction of supply in macronutrients, and in the low-latitude regions where

macronutrient supply rates are paramount (equation (B5)), all models' primary production respond in the same way. In the equatorial Pacific, our study suggests that the control on lateral iron supply is important in dictating the changes. We speculate that different parameterizations of iron chemistry and iron aeolian supply assumptions lead the CMIP5 models to respond dissimilarly here: those with strong iron limitation will have regions where increased lateral supply will lead to enhanced productivity, and those with less (or no) iron limitation will have decreased productivity. In the higher latitudes, increased growth rates can cancel out the indirect effect of lower nutrient supply. Differences in how models formulate the temperature dependence of growth (and light) will therefore lead to dissimilar balances between the effects and thus different responses in primary production. Consistent with the simulation (*All*) presented here, the CMIP5 models appear to capture the more important impact of reduced nitrate supply in the North Atlantic. These hypotheses could be assessed more quantitatively with further CMIP5 model intercomparisons.

[58] Export production is a function not only of primary production but also community composition. Models agree that smaller phytoplankton (parameterized to be less efficient at exporting organic matter) will be favored in warming scenarios [e.g., *Bopp et al.*, 2005; *Steinacher et al.*, 2010; *Marinov et al.*, 2010]. (Though we note that this widely used parameterization of strongly exporting opportunists and recycling gleaners may be too simplistic [*Richardson and Jackson*, 2007]). Indirect effects impact both primary production and functional community structure in such a way as to decrease export production on a global scale (Figure 8). Thus, decreased export production is projected by all models. Moreover, this stronger control by indirect effects could explain the more widespread regional agreement noted in CMIP5 models [*Bopp et al.*, 2013].

[59] The model results here show that there may be regions where export production increases. These are driven in some low-latitude regions by the indirect effect leading to increased lateral iron supply. And in the high latitudes, increased export occurs where the direct impact on growth rates wins out relative to the indirect effects on nutrient supply and phytoplankton functional community structural changes.

5.2. Ecological Perspective

[60] Here by including a diverse community within functional types, we have explored how ranges in phytoplankton types shift and the implication for community structure.

[61] There is a local level of winning and losing: warming and stratifying waters allow some phytoplankton types to invade a new area, out-competing the currently abundant types. The occupied ranges of some types become larger and/or shift to regions with higher nutrient supply, both of which could lead to global increase in biomass of that type. Other types will have reduced ranges and/or shifts to regions with lower nutrient supply leading to reduction in global biomass. Thus, there is a distinct difference between winning and losing locally or globally. Winning and losing on both levels can, however, be transient (Figure 4).

[62] Local community structure was altered due to shifts in the range and relative fitness of the populations. In this scenario, the local community structure was altered by more

than 50% over the course of 100 years at almost all locations relative to present-day conditions (Figure 7a). This community structure change was largely driven by temperature-related range shifts (Figure 8a) but also with an impact from reduced nutrient supplies globally. The functional biogeography of the plankton populations changes, for the most part, much less than the community structure at the phenotypical level and with a far more complex regional pattern (Figure 7b). In terms of functional groups, the changes are almost exclusively driven by changes to the limiting nutrient supply (Figure 8b).

5.3. Final Comments

[63] As a scientific community, we are keenly examining data for signs of climate-related changes in the biogeochemistry and ecology of the Earth system. In the oceans, satellite-derived changes in the area of the subtropical gyres [e.g., *Polovina et al.*, 2008], changes in chlorophyll a [e.g., *McClain et al.*, 2004; *Gregg et al.*, 2005], changes in primary productivity [e.g., *Behrenfeld et al.*, 2006], and shifts in species ranges from in situ measurement [e.g., *Beaugrand et al.*, 2002; *Beaugrand and Reid*, 2003] are suggested as signs of an altered marine environment.

[64] Here we suggest that global changes of primary and export production change will likely be only a few percent over the 21st century. Changes in broad functional classification and production rates are likely to be complex, regionally varying, and with many underlying causes. Though these changes may be biogeochemically important, they will be difficult to monitor, and it will be even more difficult to pull apart the underlying mechanisms for these changes. However, our model suggests that geographical shifts in temperature structure will dramatically change local community composition. Future monitoring of climate-induced change will have a much clearer signal at the phytoplankton population level (i.e. within functional groups), and we should expect to see significant changes in species or ecotype composition (as measured, for example, by 16S or 18S rRNA tagging) at any given location.

[65] Monitoring and understanding changes in the marine phytoplankton to a warming world is an important task, especially given the importance of these ecosystems as the base of marine food web fueling fisheries and in regulating key biogeochemical processes such as export of carbon to the deep ocean. Models, such as the one presented here, provide a "laboratory" for helping gain the necessary understanding of the complex three-dimensional system impacting the phytoplankton productivity and the reorganization of their communities.

Appendix A: Ecosystem Model Growth Equation

[66] The ecosystem model equations are almost identical to those used and provided in detail in *Dutkiewicz et al.* [2009, 2012], and we refer the reader to these papers for more details. Here we present a short discussion on the growth terms as these are crucial for our results here.

[67] Phytoplankton growth is described by equation (1):

$$\mu_j = \mu_{\max,j} \gamma_j^T \gamma_j^L \gamma_j^R \quad (\text{A1})$$

where μ_{\max_j} is the maximum growth rate of phytoplankton j , and γ_j^T , γ_j^I , and γ_j^R are the functions modulating growth due to temperature, light, and nutrient availability, respectively.

[68] Temperature modification is based on the Arrhenius function [Kooijman, 2000]:

$$\gamma_j^T = \tau \exp\left(A\left(\frac{1}{T+T_K} - \frac{1}{T_N+T_K}\right)\right) \exp(-B_j|T-T_{oj}|^b) \quad (\text{A2})$$

and sets a temperature range over which each phytoplankton j can grow (Figure 1a). Coefficients τ , A , T_K , and T_N regulate the form of the temperature modification function. T_{oj} sets the optimum temperature for each type, and B_j dictates the width of the range. There is an increase in maximum growth rate for types with higher optimum temperature as suggested by observations [Eppley, 1972; Bissinger et al., 2008]. T is the local model ocean temperature.

[69] The light sensitivity of growth rate is parameterized using the following function (modified from Platt et al. [1980]):

$$\gamma_j^I = \frac{1}{F_{\max}} \left(1 - e^{-k_{\text{par}_j} I}\right) e^{k_{\text{inhib}_j} I} \quad (\text{A3})$$

where I is the local, vertical flux of photosynthetically active radiation (PAR) and F_{\max} is chosen to normalize the maximum value of to 1 [Follows et al., 2007]. The parameter k_{par_j} defines the increase of growth rate with light at low levels of irradiation, while k_{inhib_j} regulates the rapidity of the decline of growth efficiency at high PAR, or photo-inhibition. This highly idealized parameterization of light sensitivity captures variations in optimal light intensity and their ecological implications but does not explicitly account for photo-acclimation, differences in accessory pigments, or other factors which might lead to variability in the maximum light-dependent growth factor.

[70] Nutrient limitation of growth is determined by the most limiting resource,

$$\gamma_j^R = \min(R_1^{\text{lim}}, R_2^{\text{lim}}, \dots) \quad (\text{A4})$$

where the resource R_i are nutrients phosphate, iron, silicic acid, and dissolved inorganic nitrogen. The effect on growth rate of ambient phosphate, iron, or silicic acid concentrations is represented by a Michaelis-Menton function (Figure 1c):

$$R_i^{\text{lim}} = \frac{R_i}{R_i + k_{ij}} \quad (\text{A5})$$

where the k_{ij} are half-saturation constants for phytoplankton type j with respect to the ambient concentration of nutrient i . We resolve three potential sources of dissolved inorganic nitrogen (ammonia, nitrite, and nitrate), though modeled phytoplankton may be able to assimilate ammonia only, ammonia and nitrite, or all three. Phytoplankton preferentially take up ammonia [see Dutkiewicz et al., 2009]. We do not include parameterization of nitrogen fixation in these simulations.

[71] Temperature modulation of mortality, grazing and remineralization rates, similar to that for phytoplankton growth, are based on a nondimensional factor following Kooijman [2000] though only as a function of increasing temperature with no optimal range as discussed in Dutkiewicz et al. [2012].

Appendix B: Theoretical Framework

[72] Here we recap the theoretical framework described in Dutkiewicz et al. [2009]. Consider a system (significantly simpler than the numerical model described above) of several photoautotroph (P_j , where $j = 1$ to J), nourished by a single nutrient resource (R) which has source/sink term S_R :

$$\frac{dP_j}{dt} = \mu_{\max_j} \gamma_j^T \gamma_j^I \frac{R}{R + k_{Rj}} P_j - m_j P_j \quad (\text{B1})$$

$$\frac{dR}{dt} = - \sum_{j=1}^J \mu_{\max_j} \gamma_j^T \gamma_j^I \frac{R}{R + k_{Rj}} P_j + S_R \quad (\text{B2})$$

where μ_{\max_j} is maximum growth rate for each phytoplankton type, j , γ_j^T , γ_j^I are the effect of light and temperature on growth rate, m_j is linear loss rate (that includes effects of sinking, grazing, viral lysis), and k_{Rj} is half saturation for resource uptake in Monod formulation of nutrient limitation. In this study, R could be dissolved inorganic nitrogen or iron, depending which is most limiting to growth at any location. Note that the growth term is similar to equation (1) in the numerical model but with γ_j^R explicit written out.

[73] We consider illustrative cases of this system at two extremes: steady state and spring bloom conditions.

B1. Illustrative Case 1: Equilibrium Condition

[74] Setting the left-hand side of equations (B1) and (B2), we can solve for R and P (here * indicates equilibrium solution):

$$R_j^* = \frac{k_{Rj} m_j}{\mu_{\max_j} \gamma_j^T \gamma_j^I - m_j} \quad (\text{B3})$$

$$\sum_{j=1}^J m_j P_j^* = S_R \quad (\text{B4})$$

[75] In recent studies [Dutkiewicz et al., 2009; 2012], we showed the utility of a similar framework (a version of resource competition theory [Tilman 1977; 1982]) for interpreting the relationship between organisms and their resource environment. It aided us to understand the results of the significantly more complex numerical ecosystem model similar to that used in this study. Given the equilibrium assumption, we found that it was appropriate only for the low-latitude, low seasonal regions of the model ocean and considered it only to explain the annual average results [Dutkiewicz et al., 2009; 2012]. Here we recap some essential elements and direct the reader to the earlier studies for more details.

[76] The equation for R_j^* suggests that the ambient concentration of the limiting resource is determined by characteristics of the organism including its growth rate, nutrient half-saturation constant, and mortality rate. For a system starting with several phytoplankton types, the one with the lowest R_j^* will draw the nutrient down to that value and will exclude all others in equilibrium.

[77] Assuming similar loss rates for all surviving types, $m = m_j$, equation (B4) reduces to

$$P_T^* = \frac{S_R}{m} \quad (\text{B5})$$

suggesting that phytoplankton total biomass, P_T^* , depends on the resource supply rate and the biomass loss rate.

[78] We note that this is a simplified framework, and explicit inclusion of grazers (e.g., *Armstrong 1994; Ward et al.*, 2012) or additional sink/source terms leads to nuances in these results. However, we have found [*Dutkiewicz et al.*, 2009; 2012] that this framework provides a good base to understand the far more complex numerical simulations.

B2. Illustrative Case 2: Spring Bloom

[79] In contrast to the equilibrium conditions, during initiation of the spring bloom in highly seasonal environments, nutrients are high such that in equation (B1), $R/(R+k_{Rj}) \approx 1$, and the grazer population is low ($m_j \approx 0$). In this case, the per capita growth rate is strongly regulated by growth:

$$\frac{1}{P_j} \frac{dP_j}{dt} \approx \mu_{\max j} \gamma_j^T \gamma_j^I \quad (\text{B6})$$

[80] During the spring blooms, changes to growth rate through alterations of light or temperature will be important to productivity and biomass. However, later in the season when nutrients become more limiting, the impact of changing nutrient supply may become important.

[81] **Acknowledgments.** This research was supported in part by grant DE-FG02-94ER61937 from the U.S. Department of Energy, Office of Science and by the industrial and foundation sponsors of the MIT Joint Program on the Science and Policy of Global Change (see <http://globalchange.mit.edu/sponsors/all>). This work was also funded by National Oceanic and Atmospheric Administration and the Gordon and Betty Moore Foundation. We thank N. Mahowald for making the atmospheric iron dust data available and an anonymous reviewer and Eric Sundquist for constructive comments.

References

- Armstrong, R. A. (1994), Grazing limitation and nutrient limitation in marine ecosystems: Steady state solutions of an ecosystem model with 530 multiple food chains, *Limnol. Oceanogr.*, *39*, 597–608.
- Barton, A., S. Dutkiewicz, G. Fleirl, J. Bragg, and M. J. Follows (2010), Patterns of diversity in marine phytoplankton, *Science*, *327*, 1509–1511.
- Beaugrand, G., and P. C. Reid (2003), Long-term changes in phytoplankton, zooplankton and salmon linked to climate change, *Glob. Change Biol.*, *9*, 801–817.
- Beaugrand, G., P. C. Reid, F. Ibaez, J. A. Lindley, and M. Edwards (2002), Reorganization of North Atlantic marine copepod biodiversity and climate, *Science*, *296*, 1692–1694.
- Behrenfeld, M. J., and P. G. Falkowski (1997), Photosynthetic rates derived from satellite-based chlorophyll concentration, *Limnol. Oceanogr.*, *42*, 1.20.
- Behrenfeld, M., et al. (2006), Climate-driven trends in contemporary ocean productivity, *Nature*, *444*, 752–755.
- Bissinger, J. E., D. J. S. Montagnes, J. Sharples, and D. Atkinson (2008), Predicting marine phytoplankton maximum growth rates from temperature: Improving on the Eppley curve using quantile regression, *Limnol. Oceanogr.*, *53*, 487–493.
- Bonan, G. B., et al. (2002), The land surface climatology of the Community Land Model coupled to the NCAR Community Climate Model, *J. Climate*, *15*, 3123–3149.
- Bopp, L., et al. (2001), Potential impact of climate change on marine export production, *Global Biogeochem. Cycles*, *15*, 81–99.
- Bopp, L., O. Aumont, P. Cadule, S. Alvain, and M. Gehlen (2005), Response of diatoms distribution to global warming and potential implications: A global model study, *Geophys. Res. Lett.*, *32*, L19606, doi:10.1029/2005GL023653.
- Bopp, L., et al. (2013), Multiple stressors of ocean ecosystems in the 21st century: Projections with CMIP5 models, *Biogeosci. Discuss.*, *10*, 3627–3676, doi:10.5194/bgd-10-3627-2013.
- Doney, S. C., V. J. Fabry, R. A. Feely, and J. A. Kleypas (2009), Ocean acidification: The other CO₂ problem, *Annu. Rev. Mar. Sci.*, *1*, 169–192.
- Dutkiewicz, S., A. Sokolov, J. Scott, and P. Stone, (2005a), A Three-Dimensional Ocean-Sea-ice-Carbon Cycle Model and its Coupling to a Two-Dimensional Atmospheric Model: Uses in Climate Change Studies. Report 122, Joint Program of the Science and Policy of Global Change, M.I.T., Cambridge, MA.
- Dutkiewicz, S., M. Follows, and P. Parekh (2005b), Interactions of the iron and phosphorus cycles: A three-dimensional model study, *Global Biogeochem. Cycles*, *19*, GB1021, doi:10.1029/2004GB002342.
- Dutkiewicz, S., M. J. Follows, and J. Bragg (2009), Modeling the coupling of ocean ecology and biogeochemistry, *Global Biogeochem. Cycles*, *23*, GB1012, doi:10.1029/2008GB003405.
- Dutkiewicz, S., B. A. Ward, F. Monteiro, and M. J. Follows (2012), Interconnection between nitrogen fixers and iron in the Pacific Ocean: Theory and numerical model, *Global Biogeochem. Cycles*, *26*, GB1012, doi:10.1029/2011GB004039.
- Elrod, V. A., W. M. Berelson, K. H. Coale, and K. S. Johnson (2004), The flux of iron from continental shelf sediments: A missing source for global budgets, *Geophys. Res. Lett.*, *31*, L12307, doi:10.1029/2004GL020216.
- Eppley, R. W. (1972), Temperature and phytoplankton growth in the sea, *Fishery Bull.*, *70*, 1063–1085.
- Felzer, B., D. W. Kicklighter, J. M. Melillo, C. Wang, Q. Zhuang, and R. Prinn (2004), Effects of ozone on net primary production and carbon sequestration in the conterminous United States using a biogeochemistry model, *Tellus*, *56B*, 230–248.
- Follows, M. J., S. Dutkiewicz, S. Grant, and S. W. Chisholm (2007), Emergent biogeography of microbial communities in a model ocean, *Science*, *315*, 1843–1846.
- Fyfe, J. C., and O. A. Saenko (2006), Simulated changes in the extratropical Southern Hemisphere winds and currents, *Geophys. Res. Lett.*, *33*, L06701, doi:10.1029/2005GL025332.
- Garcia, H. E., R. A. Locarnini, T. P. Boyer, and J. I. Antonov (2006), *World Ocean Atlas 2005, vol. 4, Nutrients (Phosphate, Nitrate, Silicate)*, NOAA Atlas NESDIS, 396 pp. Levitus, S. (ed), vol. 64, NOAA, Silver Spring, Md.
- Gent, P. R., and J. C. McWilliams (1990), Isopycnal mixing in ocean circulation models, *J. Phys. Oceanogr.*, *20*, 150–155.
- Gregg, W., N. Casey, and C. McClain (2005), Recent trends in global ocean chlorophyll, *Geophys. Res. Lett.*, *18*, L03606, doi:10.1029/2004GL021808.
- Kalnay, et al. (1996), The NCEP/NCAR 40-year reanalysis project, *Bull. Amer. Meteor. Soc.*, *77*, 437–470.
- Kooijman, S. A. L. M. (2000), *Dynamic Energy and Mass Budget in Biological Systems*, 424 pp., Cambridge Univ. Press, U.K.
- Large, W. G., J. C. McWilliams, and S. C. Doney (1994), Oceanic vertical mixing: A review and a model with a nonlocal boundary layer parameterization, *Rev. Geophys.*, *32*, 363–403.
- Laws, E. D. (1975), The importance of respiration losses in controlling the size distribution of marine phytoplankton, *Ecology*, *56*, 419–426.
- Liu, Y. (1996), Modeling the emissions of nitrous oxide (N₂O) and methane (CH₄) from the terrestrial biosphere to the atmosphere, Ph. D. thesis, MIT Joint Program on the Science and Policy of Global Change, Rep. 10, 219 pp.
- Luo, C., et al. (2008), Combustion iron distribution and deposition, *Global Biogeochem. Cycles*, *22*, GB1012, doi:10.1029/2007GB00296.
- Mahowald, N., and C. Luo (2003), A less dusty future? *Geophys. Res. Lett.*, *30*, 1903, doi:10.1029/2003GL01788.
- Marinov, I., S. C. Doney, and I. D. Lima (2010), Response of ocean phytoplankton community structure to climate change over the 21st century: Partitioning the effect of nutrients, temperature and light, *Biogeosciences*, *7*, 3941–3959.
- Marshall, J., A. Adcroft, C. N. Hill, L. Perelman, and C. Heisey (1997), A finite-volume, incompressible Navier-Stokes model for studies of the ocean on parallel computers, *J. Geophys. Res.*, *102*, 5753–5766.
- McClain, C., S. Signorini, and J. Christian (2004), Subtropical gyre variability observed by ocean-color satellites, *Deep-Sea Res. II*, *51*, 281–301.
- Moore, J. K., and O. Braucher (2008), Sedimentary and mineral dust sources of dissolved iron to the world ocean, *Biogeosciences*, *5*, 631.656.
- Parekh, P., M. J. Follows, and E. A. Boyle (2005), Decoupling of iron and phosphate in the global ocean, *Global Biogeochem. Cycles*, *19*, GB2020, doi:10.1029/2004GB002280.
- Platt, T., C. L. Gallegos, and W. G. Harrison (1980), Photoinhibition of photosynthesis in natural assemblages of coastal marine phytoplankton, *J. Mar. Res.*, *38*, 687–701.
- Polovina, J., E. Howell, and M. Abecassis (2008), Ocean's least productive waters are expanding, *Geophys. Res. Lett.*, *35*, L03618, doi:10.1029/2007GL031745.
- Pomeroy, L. R. (1974), The ocean's food web, a changing paradigm, *BioScience*, *24*, 499–504.
- Prinn, R., S. Paltsev, A. Sokolov, M. Sarofim, J. Reilly, and H. Jacoby (2011), Scenarios with MIT Integrated Global System Model: Significant global warming regardless of different approaches, *Clim. Change*, *104*, 51537.

- Prowe, A. E. F., M. Pahlow, S. Dutkiewicz, M. J. Follows, and A. Oschlies (2012a), Top-down control of marine phytoplankton diversity in a global ecosystem model, *Prog. Oceanogr.*, *101*, 1–13, doi:10.1016/j.pocean.2011.11.016.
- Prowe, A. E. F., M. Pahlow, and A. Oschlies (2012b), Controls on the diversity-productivity relationship in a marine ecosystem model, *Ecol. Modell.*, *225*, 167–176.
- Randall, D. A., et al. (2007), Climate models and their evaluation, in *Climate Change 2007: The Physical Science Basis. Contribution of Working Group I to the Fourth Assessment Report of the Intergovernmental Panel on Climate Change*, edited by Solomon, S., et al., Cambridge University Press, Cambridge, United Kingdom, New York, NY, USA.
- Richardson, T., and G. A. Jackson (2007), Small phytoplankton and carbon export from the surface ocean, *Science*, *315*, 838–840.
- Saba, V. S., et al. (2010), The challenges of modeling depth-integrated marine primary productivity over multiple decades: A case study at BATS and HOT, *Global Biogeochem. Cycles*, *24*, GB3020, doi:10.1029/2009GB003655.
- Sarmiento, J. L., et al. (2004), Response of ocean ecosystem to climate warming, *Global Biogeochem. Cycles*, *18*, GB3003, doi:10.1029/2003GB002134.
- Schlusser, C. A., D. Kicklighter, and A. Sokolov (2007), A global land system framework for integrated climate-change assessments. MIT Joint Program for the Science and Policy of Global Change, Rep. 147, 82 pp.
- Schmittner, A. (2005), Decline of the marine ecosystem caused by a reduction in the Atlantic overturning circulation, *Nature*, *434*, 628–633.
- Schmittner, A., A. Oschlies, H. D. Matthews, and E. D. Galbraith (2008), Future changes in climate, ocean circulation, ecosystems, and biogeochemical cycling simulated for a business-as-usual CO₂ emission scenario until year 4000 AD, *Global Biogeochem. Cycles*, *22*, GB1013, doi:10.1029/2007GB002953.
- Scott, J. R., A. P. Sokolov, P. H. Stone, and M. D. Webster (2008), Relative roles of climate sensitivity and forcing in defining the ocean circulation response to climate change, *Clim. Dyn.*, *30*, 441–454.
- Sokolov, A., and P. H. Stone (1998), A flexible climate model for use in integrated assessments, *Clim. Dyn.*, *14*, 291–303.
- Sokolov et al. (2009), Probabilistic forecast for 21st century climate based on uncertainties in emissions (without policy) and climate parameters, *J. Climate*, *22*, 5175–5204, doi:10.1175/2009JCLI2863.1.
- Steinacher, M., et al. (2010), Projected 21st century decrease in marine productivity: A multi-model analysis, *Biogeosciences*, *7*, 979–1005.
- Tagliabue, A., L. Bopp, and M. Gehlen (2011), The response of marine carbon and nutrient cycles to ocean acidification: Large uncertainties related to phytoplankton physiological assumptions, *Global Biogeochem. Cycles*, *25*, GB3017, doi:10.1029/2010GB003929.
- Taucher, J., and A. Oschlies (2011), Can we predict the direction of marine primary production change under global warming? *Geophys. Res. Lett.*, *38*, L02603, doi:10.1029/2010GL045934.
- Tegen, I., M. Werner, S. P. Harrison, and K. E. Kohfeld (2004), Relative importance of climate and land use in determining present and future global soil dust emission, *Geophys. Res. Lett.*, *31*, L05105, doi:10.1029/2003GL019216.
- Tilman, D. (1977), Resource competition between planktonic algae: An experimental and theoretical approach, *Ecology*, *58*, 338–348.
- Tilman, D. (1982), *Resource Competition and Community Structure*, 296 pp., Monogr. in Pop. Biol., vol. 17, Princeton University Press, Princeton, N. J.
- Ward, B. A., S. Dutkiewicz, O. Jahn, and M. J. Follows (2012), A size structured food-web model for the global ocean: Linking physiology, ecology and biogeography, *Limnol. Ocean.*, *57*, 1877–1891.
- Yin, J. (2005), A consistent poleward shift of the storm tracks in simulations of 21st century climate, *Geophys. Res. Lett.*, *32*, L18701, doi:10.1029/2005GL023684.